Absolute distance measurement with the MSTAR sensor

Oliver P. Lay*[a], Serge Dubovitsky[a], Robert Peters[a], Johan Burger[a], Seh-Won Ahn[b], William H. Steier[b], Harrold R. Fetterman[c], Yian Chang[c]
[a]Jet Propulsion Laboratory, California Institute of Technology, 4800 Oak Grove Drive, Pasadena CA 91109
[b]Department of Electrical Engineering, University of Southern California, Los Angeles, CA 90089
[c]Pacific Wave Industries, 10390 Santa Monica Blvd, Suite 100, Los Angeles, CA 90025

ABSTRACT

The MSTAR sensor (Modulation Sideband Technology for Absolute Ranging) is a new system for measuring absolute distance, capable of resolving the integer cycle ambiguity of standard interferometers, and making it possible to measure distance with sub-nanometer accuracy. The sensor uses a single laser in conjunction with fast phase modulators and low-frequency detectors. We describe the design of the system - the principle of operation, the metrology source, beam-launching optics, and signal processing - and show results for target distances up to 1 meter. We then demonstrate how the system can be scaled to kilometer-scale distances.

Keywords: Absolute metrology, distance measurement

1. INTRODUCTION

High-precision non-contact measurements of distance are required in many areas of science and engineering. In addition to well-established uses of distance metrology in optical figure sensing, high-precision metrology is also used in the semiconductor industry for lithography, mask/wafer inspection and measurement, and process control. Metrology is also used in general precision-positioning applications, such as measurement and calibration of high-resolution motions and in high-precision machining. Of particular interest for this paper is the use of precision optical distance metrology for optical pathlength control in ground- and space-based stellar interferometers. To be practical for these applications, a metrology gauge must be able to operate with target distances anywhere from a few centimeters to a kilometer.

Laser interferometry is an established method for displacement measurement; sub-nanometer precision has been achieved[1,2], but absolute distance is ambiguous, because of the inherent half-wavelength (~0.5 um) ambiguity range. To determine the target distance with high accuracy the ambiguity range of the fine interferometric stage must be resolved with an additional coarse gauge or gauges. The set of gauges used to resolve the fine sensor ambiguity range is often referred to as absolute metrology. The range accuracy of the absolute metrology stage must be better than the ambiguity range of the relative fine stage; resolving a half-wavelength ambiguity range of 0.5 μm requires a 1σ absolute range accuracy of ~0.1 μm (peak-valley error ~0.5 μm), significantly beyond the existing capability.

A number of methods exist for the unambiguous measurement of target distance. The most common method, based on the time-of-flight[3] of emitted pulses, cannot achieve the necessary accuracy, because a timing accuracy of 0.6 femtoseconds is required for a range accuracy of 0.1 μm. Other techniques, such as intensity-modulated optical beam[4,5], frequency-modulated optical beam, and two-color interferometry[6] are used where higher accuracy is required. The rms accuracy is currently limited to ~5 μm, although there are examples of higher accuracy in more restricted applications, usually at very short target distances[7-10].

The methods relying on the generation and detection of high-frequency optical carrier modulation suffer from the low responsivity of the high-speed photodetectors required for their operation, and the need for high-speed signal processing electronics.

* oliver.p.lay@jpl.nasa.gov; phone 1 818 354-2521; fax 1 818 393-4950

Two-color interferometry is the most promising approach, in which two laser interferometer measurements are made at different laser wavelengths. Differencing these measurements is equivalent to having a laser interferometer with a much longer synthetic wavelength[6]. High accuracy over large distances imposes four requirements: (1) the coherence length of the laser must be longer than the round-trip distance to be measured; (2) the laser wavelength must be known to the accuracy needed for the measurement (10 nm accuracy at 100 m requires 10^{-10} wavelength knowledge); (3) the combination of synthetic wavelength and phase resolution must be sufficient to achieve the 0.1 μm accuracy; and (4) the synthetic wavelength must be known with high accuracy (0.1 ppm for 1 m distance, 0.01 ppm for 10 m distance, etc.). This combination has not been achieved with existing lasers.

In this paper we discuss a new architecture that overcomes the existing limitations, and experimentally demonstrate unambiguous measurements with resolution sufficient to resolve the integer cycle ambiguity. The technique, Modulation Sideband Technology for Absolute Ranging (MSTAR), implements a two-color metrology system using a single narrow-linewidth, frequency-stabilized laser; the multiple wavelengths are produced as phase modulation sidebands using fast integrated-optics modulators. The two-color approach avoids the need for the fast photodetectors and signal processing required for other RF modulation schemes[4,5]. Another important benefit of the MSTAR system is that the fine relative gauge is an integral part of the system, giving seamless integration of the absolute and fine (sub-nanometer) relative stage into a single high absolute accuracy sensor.

2. THE MSTAR SYSTEM

2.1. Overview

In this section we describe the basic MSTAR configuration. The following sections then provide more details for the different parts of the system.

The system is shown in Fig. 1. The laser light, frequency ν, is split into the Measurement and Local arms. In the Measurement arm the laser frequency is up-shifted by f_M, and a sinusoidal phase modulation $\Delta\Phi \sin(2\pi F_M t)$ is applied, producing a series of sidebands spaced by $\pm F_M$, $\pm 2F_M$, $\pm 3F_M$, ... Similar modulation, using slightly different frequencies as indicated in Fig. 1, is applied to the Local arm. The resulting optical spectrum for the Measurement and Local beams is shown in Fig. 1b (higher order sidebands have been omitted for clarity). The upper and lower sidebands correspond to the two wavelengths of a two-color interferometer. The electric field amplitude of the kth sideband is given by the appropriate Bessel function: $J_k(\Delta\Phi)$. Weak phase modulation gives a dominant carrier frequency and weak first sidebands. As the modulation is raised, the sidebands increase in size and number and the carrier level is depressed. It is also possible to use intensity modulation instead of phase modulation to generate the sidebands; the analysis below will be the same for each case.

The Measurement beam is collimated and directed towards the target retroreflector. The outer part of the beam is returned by the Reference mirror. It is attenuated on passing through the Measurement and Local beamsplitters before being deflected to the Reference photodetector. The central core of the Measurement beam propagates to the Target retroreflector, returns through the hole in the Reference mirror and ends up at the Target photodetector. The Local beam takes a shorter route to the two detectors, as shown in Fig. 1a.

The Measurement and Local beams mix at the detectors, generating the down-converted frequencies shown in Fig. 1c (the low-frequency detectors are not sensitive to the high-frequency mixing products between different sidebands). The second sidebands, not shown in Fig. 1c, would be found at 10 kHz and 170 kHz. The choice of modulation frequencies is such that the spectrum at the output of the detectors (Fig. 1c) is a highly compressed version of the optical spectrum (Fig. 1b), with a spacing of 40 kHz instead of 40 GHz. These low frequency signals greatly simplify the signal processing, and enable the use of much more sensitive low-frequency photodetectors. The photodetector outputs are bandpass filtered to isolate the sinusoids for the carrier, upper, and lower sidebands. The details are described in the signal processing section below.

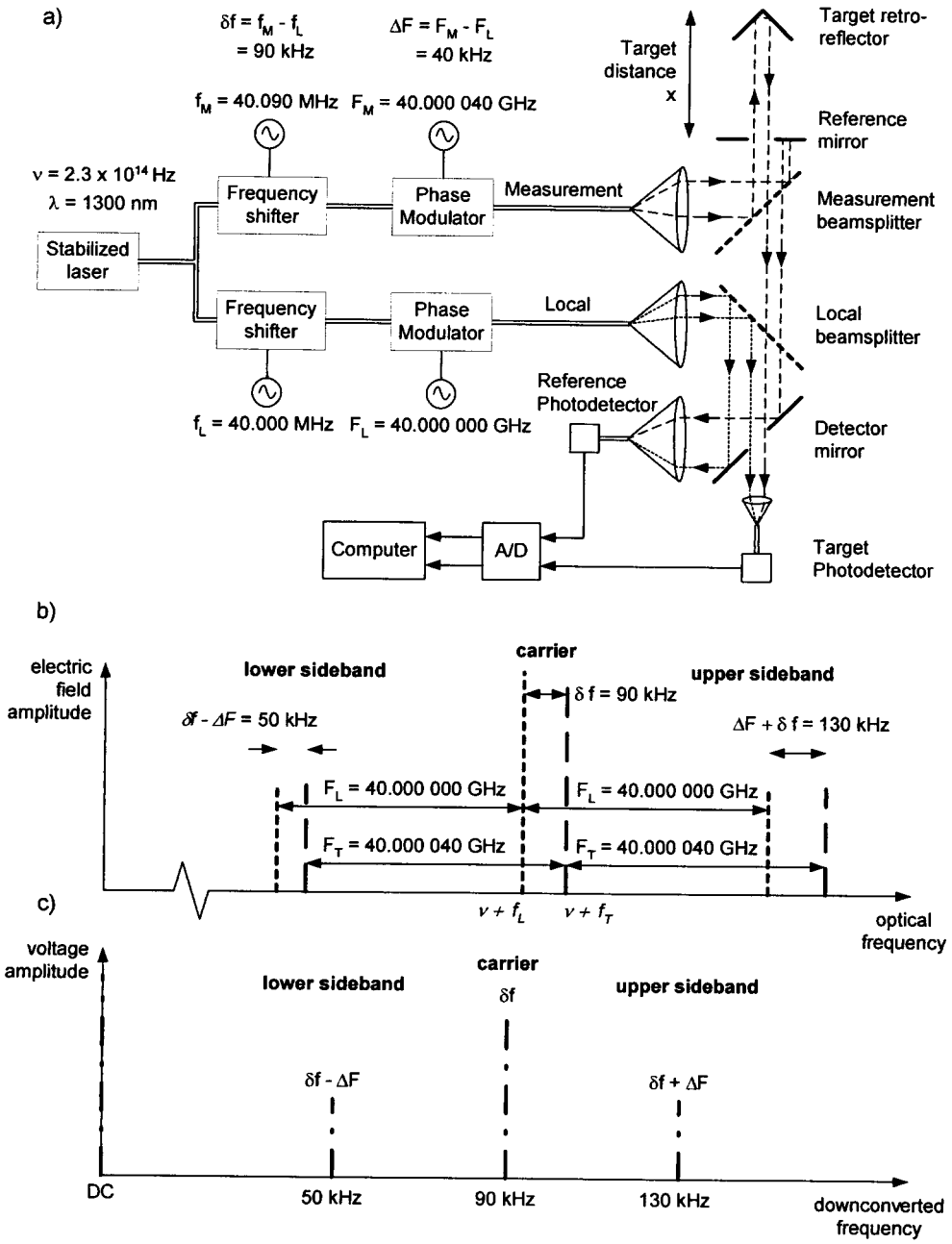

Figure 1: (a) Schematic of the *MSTAR* system. The distance to be measured, *x*, lies between the reference mirror and the target retro-reflector. (b) Optical spectrum before photo-detection. Long-dash = measurement beam; short-dash = local beam (c) Spectrum of electrical signals after photo-detection.

Consider a virtual plane *Z*, lying between the Local beamsplitter and the Detector mirror in Fig. 1a, normal to the propagation direction. We define the phase of the *k*th sideband of the outer (Reference) part of the Measurement beam at this point to be $\varphi^{(Z)}_{M,R,k}\big|_0$ at time $t = 0$. The phases of the inner (Target) part of the Measurement beam as it passes through plane *Z*, and for the Local beam, are given by

$$\phi_{M,T,k}^{(Z)} = \phi_{M,R,k}^{(Z)}\Big|_0 + (\nu + f_M + kF_M)\left(t - \frac{2x}{c}\right) \tag{1}$$

$$\phi_{L,k}^{(Z)} = \phi_{L,k}^{(Z)}\Big|_0 + (\nu + f_L + kF_L)t. \tag{2}$$

In order to avoid the constant repetition of 2π in the equations, all phases are in *cycles* (1 cycle=2π radians). Most symbols are defined in Fig. 1a, and c is the speed of light in vacuum (see section on signal processing for modifications needed when experiment is carried out in air). At the Target detector, the difference in phase between the Measurement and Local beams is given by

$$\begin{aligned}\Delta\phi_k^{(T)} &= \phi_{M,T,k}^{(T)} - \phi_{L,k}^{(T)} = \left\{\phi_{M,R,k}^{(Z)}\Big|_0 + (\nu + f_M + kF_M)\left(t - \frac{2x}{c} - \tau_{TZ}\right)\right\} - \left\{\phi_{L,k}^{(Z)}\Big|_0 + (\nu + f_L + kF_L)(t - \tau_{TZ})\right\} \\ &= -(\nu + f_M + kF_M)\left(\frac{2x}{c}\right) + \left(\phi_{M,R,k}^{(Z)}\Big|_0 - \phi_{L,k}^{(Z)}\Big|_0\right) + (\delta f + k\Delta F)(t - \tau_{TZ})\end{aligned} \tag{3}$$

where τ_{TZ} is the propagation delay between plane Z and the Target photodetector. The first term contains the distance information, the second is an offset, and the third specifies the RF frequency at the output of the detector (δf and ΔF are defined in Fig. 1a). At the Reference detector we obtain the result

$$\Delta\phi_k^{(R)} = \phi_{M,T,k}^{(R)} - \phi_{L,k}^{(R)} = \left(\phi_{M,R,k}^{(Z)}\Big|_0 - \phi_{L,k}^{(Z)}\Big|_0\right) + (\delta f + k\Delta F)(t - \tau_{RZ}). \tag{4}$$

The difference in phase between the kth sideband from the Target detector and the kth sideband from the reference detector is

$$\Delta\phi_k = \Delta\phi_k^{(R)} - \Delta\phi_k^{(T)} = (\nu + f_M + kF_M)\left(\frac{2x}{c}\right) + (\delta f + k\Delta F)(\tau_{TZ} - \tau_{RZ}). \tag{5}$$

The second term is negligible. For example, if there is a 1 cm difference in the path lengths from Z to Target and Local detectors, and the RF frequency ($\delta f + k\Delta F$) = 100 kHz, then the second term corresponds to 3×10^{-6} cycles of phase.

For the carrier ($k = 0$, RF frequency δf), ignoring the second term,

$$\Delta\phi_0 = (\nu + f_M)\left(\frac{2x}{c}\right). \tag{6}$$

The integer number of cycles in the phase measurement is unknown and the resulting estimate of x is ambiguous:

$$x_{car} = \frac{c}{2(\nu + f_M)}(\Delta\phi_0 \pm m) = L(\Delta\phi_0 \pm m) \tag{7}$$

where m is an integer. We will refer to this as the carrier length estimate. The ambiguity length L is approximately half the laser wavelength. The 1σ-precision of the length measurement (σ_x) depends on the precision of the phase difference: $\sigma_x = L\sigma_{\Delta\phi}$. This carrier measurement is equivalent to a standard heterodyne metrology gauge.

In addition to making this sub-nanometer measurement, MSTAR uses the sidebands to determine the number of integer cycles m in Eq. 7. The first upper sideband has a phase difference of $\Delta\phi_1 = (\nu + F_M + f_M)(2x/c)$ between Target and Reference outputs. The first lower sideband gives $\Delta\phi_{-1} = (\nu - F_M + f_M)(2x/c)$. Differencing gives

$$\Delta\phi_{+1} - \Delta\phi_{-1} = 2F_M\left(\frac{2x}{c}\right). \tag{8}$$

The resulting estimate of the distance, which we will refer to as the sideband length estimate, is

$$x' = \frac{c}{4F_M}(\Delta\phi_{+1} - \Delta\phi_{-1} \pm n) = L'(\Delta\phi_{+1} - \Delta\phi_{-1} \pm n) \tag{9}$$

analogous to Eq. 7, but with a substantially longer ambiguity length, $L' = c/(4F_M)$, and precision $\sigma_x' = L'\sqrt{2}\sigma_{\Delta\phi}$. The synthetic wavelength is $c/2F_M$.

As an example of how measurement of x' can be used to resolve ambiguity m consider the frequencies shown in Fig. 1. The carrier phase ambiguity length is L = 0.65 μm. With a phase resolution of $\sigma_{\Delta\phi}$ = 5 x 10^{-5} cycles (0.3 mrad), σ_x = 30 pm. The sideband combination has L' = 1.875 mm and σ_x' = 0.12 μm, sufficient to resolve L (and therefore m) at a high level of probability. The remaining ambiguity (n) can be resolved by switching to a lower phase modulation frequency. Switching to a phase modulation frequency of 30 MHz gives L'' = 2.5 m and σ_x'' = 0.18 mm, sufficient to resolve n. This is illustrated schematically in Fig. 2.

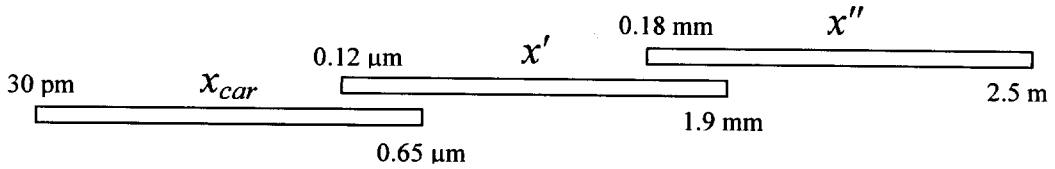

Figure 2: Schematic representation of the 3 stages of length measurement given in the text. The left end of each bar indicates the resolution of the measurement; the right end indicates the ambiguity length. Lower resolution stages are easily added.

The key step is being able to resolve the number of integer optical wavelengths m, which requires $\sigma_x' \ll \lambda/2$. This condition is equivalent to $\sigma_{\Delta\phi} / F_M \ll \sqrt{2} / \nu$. Both high phase modulation frequency F_M and excellent phase resolution $\sigma_{\Delta\phi}$

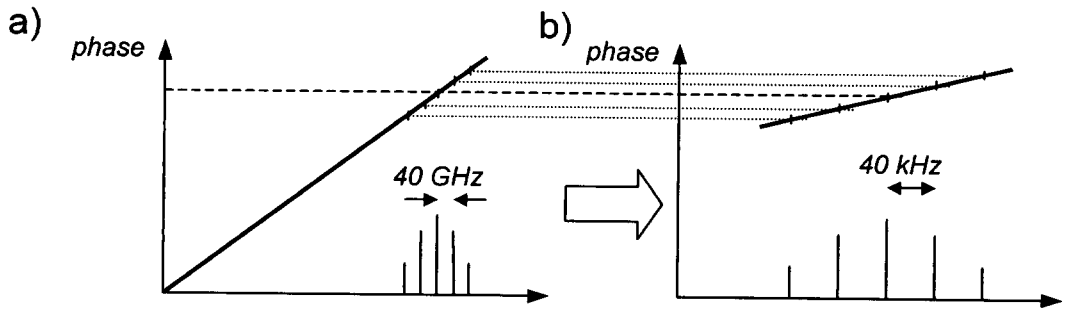

are needed to meet this. Once met, a further increase in modulation frequency allows a relaxation of the phase resolution, and vice versa.

Figure 3: (a) By measuring the phase for the carrier and modulation sidebands, MSTAR effectively determines the group delay (the local slope of the phase vs. optical frequency curve). (b) Down-conversion by the modulated local oscillator maps the optical spectrum to the detector output spectrum, with the frequency scale compressed by a factor of 1000 (using the frequencies shown in Fig. 1).

Another way to conceptually understand the MSTAR operation is illustrated Fig. 3. Phase measurement using the carrier and a number of sidebands enables the measurement of the phase gradient vs. optical frequency, which is essentially the group delay. The detector output spectrum looks the same as the optical spectrum, but is heavily compressed in frequency. In the example shown, the phase gradient measured at the detector output is 1000 times the phase gradient in the optical spectrum.

2.2. Metrology source

The metrology source includes the stabilized laser, optical fiber, frequency shifters and phase modulators shown in Fig. 1a. The laser is a Nd:YAG system with linewidth of 10 kHz at 1.32 μm, from Lightwave Corporation. The very narrow linewidth has a coherence length of ~30 km, which is important for long-range applications. The laser wavelength is measured against a HeNe reference laser using a Burleigh WA-1500 wavemeter (accuracy ~0.1 ppm), and a control loop provides feedback to stabilize the laser. The output is coupled into single-mode polarization-maintaining

(PM) optical fiber at a level of 200 mW. A fiber splitter sends laser light to the Measurement and Local arms, where the optical frequency is up-shifted by ~40 MHz using acousto-optic modulators, and then fed into high-frequency phase modulators operating at ~40 GHz.

The phase modulators are polymer-based integrated optics devices[11] built by USC and Pacific Wave. Polymer-based modulators are more efficient than $LiNbO_3$ devices at high frequencies due to a better velocity match between the RF and optical waves. The 2 cm long devices have a V_π of 3 V at low frequency, and a V_π of 12-16 V at 40 GHz. The modulators were packaged in N_2 to improve the long-term photo-stability. The phase modulators are driven at ~40 GHz by a pair of Agilent 83650B synthesizers (accurate to ~0.1 ppm), with MMIC amplifiers providing an additional 40 dB of gain. With +23 dBm of RF input power, the first sidebands are 12 dB down from the carrier. The packaged modulators have a fiber-to-fiber insertion loss of ~12dB.

If PM optical fiber is used throughout the metrology source, then the optical path length through the system depends on the polarization state. To avoid this problem, a length of polarizing (PZ) single-mode optical fiber is used between the phase modulators and the collimators, providing a true single mode.

2.3. Beam launcher optics

The MSTAR system described above has 4 paths that the signals can take, as depicted in Fig. 1a. Light taking any other path to the detectors will cause an error. The phase resolution of $\sigma_{\Delta\phi} = 5 \times 10^{-5}$ cycles (0.3 mrad) requires that the total optical power in the error paths is down by ~70 dB ($20\log_{10}0.0003$). Error paths include multiple back-reflections in a single path, and leakage between the inner and outer parts of the Measurement beam. The beam launcher optics, shown in Fig. 4 were designed to minimize these effects.

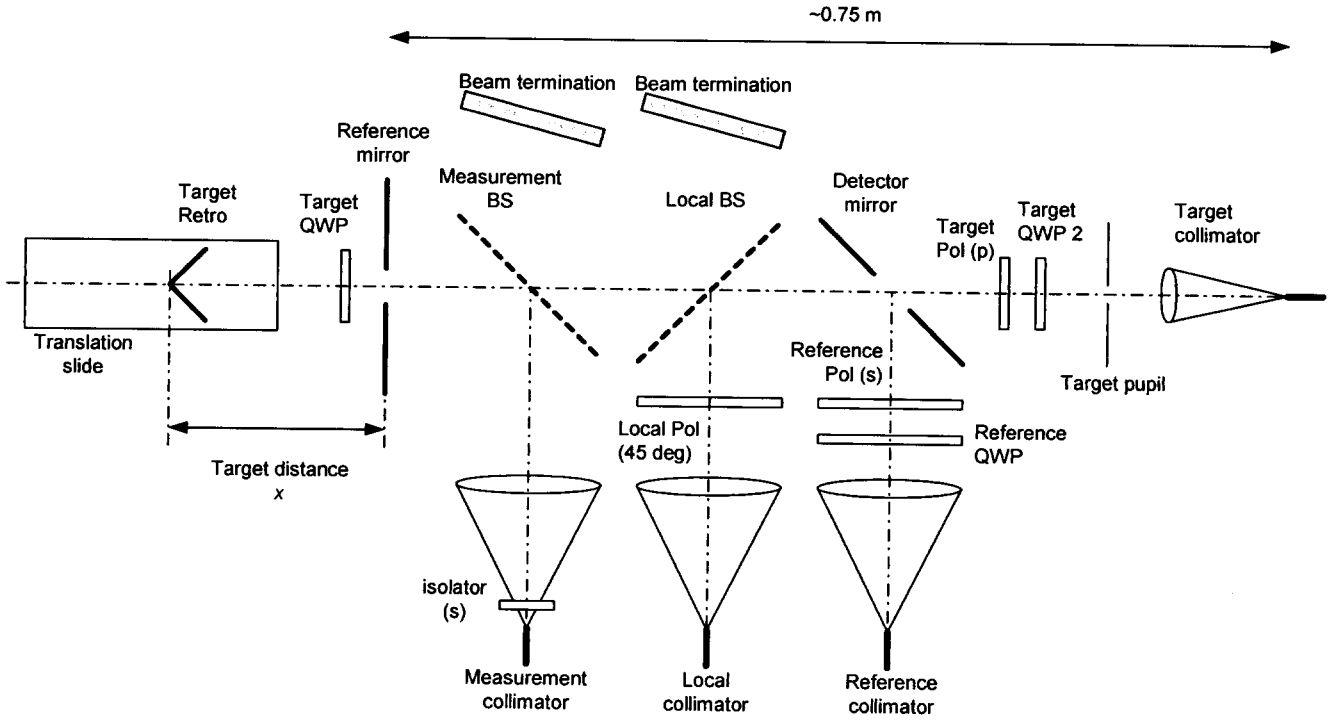

Figure 4: Beam launcher optics. "s" and "p" indicate the direction of polarization (s is normal to the page, p is in the plane of the page, 45 deg is midway between the two). Pol = Polarizer, QWP = Quarter-Wave Plate.

The main difference compared to the schematic in Fig. 1a is the addition of polarizing optics to provide a second level of isolation. Light from the Measurement arm passes through a ferrite isolator before collimation, polarizing the light in the s direction. The isolator suppresses the error path formed by back-reflection from the Reference mirror followed by back-reflection from the tip of the Measurement collimator. The collimators are 2-inch achromatic doublets. The

Measurement beam reflected from the Reference mirror is s-polarized, passing through the Reference Polarizer to the Reference Collimator. Two things prevent this light from reaching the Target collimator: the Target pupil is under-sized compared to the hole in the Reference mirror, and the s-polarization is blocked by the Target polarizer. The inner part of the Measurement beam passes twice through the Target Quarter-Wave Plate, returning as p-polarized light. This light is prevented from reaching the Reference collimator by a combination of the over-sized hole in the Detector mirror, and the Reference polarizer, which does not transit the p-polarization. The Reference and Target Quarter-Wave Plates form isolators with their respective polarizers, and suppress the back-reflections from the fiber tips of the Reference and Target collimators. The Local beam is polarized at a 45-degree angle, so that it couples to both the Target and Reference detectors. The Target retro-reflector is mounted on a manual translation stage, 1 m in length.

The current breadboard beam launcher was intended for demonstrating performance in the lab. The use of 2-inch optics and adjustable mounts for most components makes the beam launcher too large to be practical in many applications. The presence of the Target Quarter-Wave Plate in the target path also complicates the measurement of x, since we must correct for the increased electrical length. The next version of the beam launcher will be much smaller, and the use of Angle-Polished fibers may avoid the need for the polarizing optics.

2.4. Signal processing

Achieving a phase resolution of $\sigma_{\Delta\phi} = 5 \times 10^{-5}$ cycles (0.3 mrad) requires some care in the processing of the signals. The detectors are standard battery-operated New Focus 2011 models, which operate up to a bandwidth of 300 kHz and provide switchable levels of gain. The signals are digitized with a Gage 2-channel 14-bit A/D card, sampling at a rate of 500 kHz, such that 2^{16} samples per channel are obtained in a total measurement time of $t_m = 0.13$ s.

The phase as a function of time for each line in the RF spectrum for each detector output is obtained with the following procedure. (1) Each time series is Fourier transformed. (2) The negative frequencies are discarded. (3) For each carrier/sideband in the spectrum, a block of channels centered on the nominal line frequency is extracted. (4) This segment of the spectrum, shifted to DC, is then Fourier transformed to give a complex function in the time domain. The complex argument of this function is the phase of the sideband over the 0.13 s period, $\Delta\phi_k^{(T)}$ or $\Delta\phi_k^{(R)}$. (5) For each carrier/sideband we difference the phases obtained for the Target and Reference detectors, $\Delta\phi_k = \Delta\phi_k^{(T)} - \Delta\phi_k^{(T)}$. The process is essentially a Hilbert transform[12] of the original time series, with additional filtering and down-conversion to isolate the different spectral components, and is much more robust than a zero-crossing approach to phase measurement.

Differencing the phases for the different sidebands gives distance as a function of time, as shown by Eq. 9. If the target is stationary, we can simply average over the time series to get distance. If the target is moving, we can use the technique of "carrier-aided smoothing", first developed for Global Positioning System applications[13]. The phase difference $\Delta\phi_0$ obtained for the carrier (or for any one of the sidebands) provides an accurate estimate of the change in distance over time t_m:

$$\Delta x_0(t) = \left(\Delta\phi_0(t) - \Delta\phi_0(0)\right)\frac{\lambda_0}{2\pi}, \tag{10}$$

where λ_0 is the optical wavelength of the carrier, and $t = 0$ corresponds to the start of the measurement. This can be subtracted from the sideband length estimate before averaging:

$$\overline{x'(0) = x'(t) - \Delta x_0(t)}. \tag{11}$$

The result is an estimate of the distance to the target at the start of the measurement period t_m. This technique makes possible the use of arbitrarily long coherent integration times to boost the signal-to-noise ratio, in the presence of vibration and motion.

We can now solve for the integer number of cycles in Eq. 7:

$$m = \mathrm{rnd}\left(\frac{2x'}{\lambda_0} - \Delta\phi_0\right), \tag{12}$$

where rnd denotes rounding to the nearest integer, and $0 < \Delta\phi_0 < 1$. This resolves the ambiguity in the carrier length estimate:

$$x_{car} = \frac{c}{2(\nu + f_M)}\left[\Delta\phi_0 + \mathrm{rnd}\left(\frac{2x'}{\lambda_0} - \Delta\phi_0\right)\right]. \tag{13}$$

The previous results all apply to the use of MSTAR to measure a length in vacuum. A few modifications are needed for operation in air. The physical length is

$$x = \frac{c}{n_p}\tau_p = \frac{c}{n_g}\tau_g, \tag{14}$$

where c is the speed of light in vacuum, n_p and n_g are the phase and group refractive indices, and τ_p and τ_g are the phase and group delays, respectively. We also define the electrical phase and group delay lengths as $x_p = c\,\tau_p$ and $x_g = c\,\tau_g$. In a non-vacuum medium, the carrier length estimate (Eq. 7) is an estimate of the electrical phase delay length x_p, as is the truth estimate (Eq. 16), whereas the sideband length estimate (Eq. 9) is an estimate of the electrical group delay length x_g. Therefore a correction must be applied to the sideband length estimate to compensate for the difference in the refractive indices:

$$x_{cor}' = \frac{n_p}{n_g}\left(1 - 1.79\times10^{-6}\right)x' \ . \tag{15}$$

The ratio of refractive indices is computed using Ciddor's model[14] for dispersion in air, for a pressure of 1 atm, temperature of 20 deg C and a relative humidity of 30%, at a wavelength of 1320 nm. This corrected value should be substituted for x' in the previous equations of this section, and is used for the results presented in section 3. The correction amounts to ~2 μm per meter of length measured.

2.5. Verification

In order to verify the accuracy of MSTAR, measurements were compared with a phase meter developed for the Space Interferometry Mission (SIM)[15]. This phase meter, not shown in Fig. 1a, is connected to the outputs of the photodetectors, in parallel with MSTAR data acquisition. It first converts the heterodyne sine wave to square waves to reduce amplitude dependence, then measures the time between the signals on the measurement and reference channel. The phase meter also counts the integer number of cycles to track displacements over large distances. This phase meter is incompatible with the MSTAR modulation; the next section describes how it is employed.

2.6. Measurement sequence

The MSTAR experiment is run using automatically using the LabView environment. Each measurement with the MSTAR system consists of the following steps:

1. Turn on low-frequency phase modulation with $F_M = 30.040$ MHz and $F_L = 30.000$ MHz
2. Obtain digitized time series simultaneously for the Target and Reference detector outputs and process to give a coarse distance estimate
3. Switch from low-frequency phase modulation to high frequency modulation with $F_M = 40.000{,}040$ GHz and $F_L = 40.000{,}000$ GHz
4. Obtain digitized time series simultaneously for the Target and Reference detector outputs and process to give a fine distance estimate
5. Turn off the phase modulation
6. Measure the differential phase with the verification phasemeter
7. Move the target retro-reflector to the desired new position, with the verification phasemeter counting fringes
8. Calculate the change in position from the number of fringe counts from the verification phasemeter. Add this to previous displacements to determine the displacement relative to the original starting position
9. Go to step 1

Note that the MSTAR estimate of the target position is calculated independently at each target position, and the phase modulation is turned off while the target is being moved. When the phase modulation is turned on, the verification phasemeter output is no longer valid – this is why the displacement of the target must be calculated as a sum over a

series of steps, each of which is measured with the phase modulation off. The independent "true" position is then given by

$$x_{TRUTH} = x_{START} + \sum_i \Delta x_i = x_{START} + \Delta x_{TRUTH}, \quad (16)$$

where x_{START} is the unknown starting position and Δx_i are the measured lengths of each step.

3. RESULTS

Three types of experiment were conducted to validate performance: (I) a displacement test, (II) a stability test, and (III) a zero test.

(I) *Displacement test.* From an arbitrary starting position the target was moved in small increments along the track. At each position, MSTAR generated a position, x_{MSTAR}, based only on the sideband difference phases. Equation 9 shows that this measurement depends only on the phase modulation frequency (tied to the synthesizer's frequency reference), and is independent of the laser wavelength. The 'truth' measurement depends only on the accuracy of fringe counting by the independent verification phase meter, and the wavelength of the laser light (tied to the wavelength of the HeNe reference laser). An example set of data is shown in Fig. 5, with the MSTAR distance plotted against the 'truth'. Also shown is the residual, $\sigma'_x = x_{MSTAR} - \Delta x_{TRUTH} - x_{START}$ (note that x_{START} is equated to the first value of x_{MSTAR}, so that $\sigma'_x = 0$ for the first point by definition). The standard deviation of this residual (0.12 μm) is typical of the results obtained, and demonstrates that MSTAR can measure *displacements* (as opposed to absolute position) with the accuracy necessary to resolve the number of integer cycles *m*.

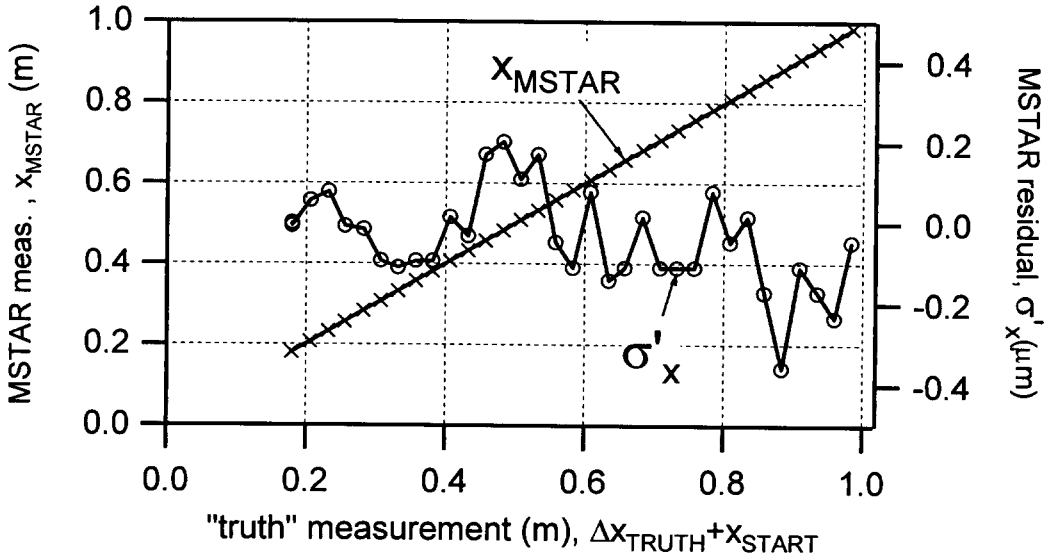

Figure 5: MSTAR absolute measurement vs 'true' displacement from start point (based on fringe counting). The residual error, $\sigma'_x = x_{MSTAR} - \Delta x_{TRUTH} - x_{START}$ is overlaid.

(II) *Stability test.* This test was conducted in the same way as the displacement test, except the target was not deliberately moved (small thermal motions were tracked with the truth measurement). Over a 3-hour period, the standard deviation of the residual was 0.05 μm, demonstrating that MSTAR is stable and calibratable.

(III) *Zero test.* It was not possible to extend the displacement test down to zero separation between the reference mirror and the vertex of the target retro-reflector. This is because the target retro-reflector and target quarter-wave plate were too large to fit through the small (~5 mm) hole in the reference mirror (Fig. 4). The annular reference mirror was instead replaced by a standard plane mirror, giving a target surface that is co-planar with the reference. The MSTAR measurements were consistent with zero to within 0.2 μm.

The tests show that MSTAR's sideband length estimate measures displacements with accuracy sufficient to resolve the integer-cycle ambiguity. It also measures the absolute zero position correctly. It should be noted that this combination of tests does not rule out the possibility of an anomaly in the MSTAR reading between zero and the start point of the displacement test (~18 cm). To exclude this possibility, we are planning to test the system with a much smaller target retro-reflector that will fit through the hole in the annular reference mirror. A white light interferometer will be used to establish when the vertex of the retro-reflector is coincident with surface of the reference mirror. This will establish $x_{START} = 0$ for the fringe counting verification measurement.

The tests above only address the accuracy of the sideband length estimate (Equ. 9). The MSTAR system simultaneously generates a carrier length estimate (Equ. 7) which, in combination with the sideband length estimate (Equ. 13), has subnanometer accuracy. This level of performance was not tested in the experiments.

4. EXTENSION TO LONG-RANGE TARGETS

The MSTAR system has only been demonstrated in the laboratory for stationary targets, at ranges of up to 1 m. Operation at longer range imposes additional requirements on the system performance:

1. The coherence length of the laser source must be larger than the round-trip optical path to the target.
2. The uncertainty in the laser wavelength must be reduced.
3. The uncertainty in the RF modulation frequency must be reduced in order to resolve the integer cycle ambiguity.
4. The system must accommodate the increased photon noise due to the weaker return signal.
5. The weaker target return signal is more prone to leakage and multi-path effects, requiring increased optical isolation.

Each of these items is addressed below, followed by a brief section on moving targets.

4.1. Coherence length

As noted in section 2.2, the Lightwave NPRO laser has a linewidth of 10 kHz. The associated coherence length of 30 km is therefore sufficient in principle for target distances of up to 15 km.

4.2. Laser wavelength uncertainty

Obtaining range accuracy σ_x at range x, requires knowledge of the laser wavelength to a fraction σ_x/x. For example, if x = 100 m and σ_x = 10 nm, then the wavelength must be known with fractional uncertainty less than 10^{-10}. High accuracy measurements over long distances will require a frequency stabilized laser source. Since it is the knowledge of the laser frequency that is important, and not just the frequency stability, commonly used Fabry-Perot cavity references cannot be relied upon, since the cavity is prone to long-term drift. Therefore, we must use an atomic or molecular resonant transition as a frequency reference.

The 1.319-μm wavelength NPRO laser currently used for MSTAR has a frequency of 2.3×10^{14} Hz. In order to achieve a position uncertainty of 10 nm over a target separation of 100 m, we must know the laser frequency to within 23 kHz. We have investigated a variety of frequency standards and locking techniques that could achieve this level of frequency accuracy. We believe the best frequency standards for MSTAR would be either molecular iodine or methane. Methane may be used directly with the laser wavelength of 1.319 μm, whereas iodine would require the laser frequency to be doubled to a give a wavelength of 659 nm.

Locking a doubled 1319 nm laser to iodine has already been demonstrated[16] with frequency uncertainty of 2.4×10^{-10} (55 kHz). The frequency stabilization system locks on the Lamb-dip[17] at the center of the Doppler broadened absorption profile, using am FM spectroscopy technique similar to that used in common Pound-Drever-Hall[18] locking systems. We believe that similar performance may be achieved using methane without the need for frequency doubling.

4.3. Modulation frequency uncertainty

Resolving the integer-cycle ambiguity requires a range resolution of ~100 nm for the sideband length estimate. The phase modulation frequency must therefore be known with fractional uncertainty less than (100 nm / x). For x = 100 m, the knowledge requirement is 10^{-9}, which is easily met by a number of frequency standards[19]. Compact Rubidium-based systems have an accuracy of ~5×10^{-11}; laser-cooled Cesium systems approach 10^{-15}.

4.4. Increased photon noise

As the photon rate for the return signal is reduced, shot noise becomes the dominant source of random noise in the system. The photon rate can be increased by using a higher power laser, or by increasing the diameter of the target beam and retro-reflector to minimize diffraction losses. This is not necessary, however, since the coherent integration time can be increased arbitrarily, even in the presence of vibration and target motion, using the carrier-aided smoothing technique (section 2.4).

4.5. Increased leakage

The weaker return signal is also more susceptible to multi-path effects and leakage from the reference part of the beam (section 2.3). Higher laser power and longer integration times are not going to help with this systematic error. In the far-field limit, the optical return loss for the target beam is proportional to d^4, where d is the outgoing beam diameter. A large target beam is therefore highly advantageous. The isolation properties of the beam launcher are also likely to be improved by going to a more compact design that minimizes the effects of diffraction, and uses angle-polished fibers to minimize back-reflections.

In summary, we do not believe there are serious obstacles to scaling the performance of MSTAR to ranges of 100 m or more. Of the items listed above, the last one probably warrants the most attention, and will be the subject of further investigation.

5. SUMMARY

We have described the architecture and operation of the MSTAR sensor, a new distance-measuring system based on the use of fast phase modulators. The target modulator generates carrier sidebands – the multiple 'colors' of an absolute metrology system – which are down-converted by the sidebands produced by the local modulator, enabling low-speed detection and signal processing. The beam-launcher is optimized to minimize cross-talk and leakage between the beams, so that we can measure phase differences with an accuracy of 0.3 mrad. The combination of high-speed modulation (40 GHz) and high phase resolution lead to an absolute range resolution of ~100 nm, sufficient to resolve the integer cycle ambiguity of standard laser metrology systems (also an integral part of the MSTAR sensor), and making possible long-range distance measurement with unprecedented accuracy. Although MSTAR has only been demonstrated over distances of up to 1 m, we show that there are no major obstacles to achieving sub-micron performance over much longer ranges.

The work described in this paper was performed at the Jet Propulsion Laboratory, California Institute of Technology, under contract with the National Aeronautics and Space Administration.

REFERENCES

1. N. Bobroff, "Recent advances in displacement measuring interferometry," *Meas. Sci. Technol.*, vol. 4, pp. 907-926, 1993.
2. F. Zhao, "Demonstration of sub-Angstrom cyclic non-linearity using wavefront-division sampling with a common-path laser heterodyne interferometer", American Society of Precision Engineering Annual Meeting, Arlington, VA, Nov 10-15 (2001)
3. O. Bock, "Relative positioning precision of the wide-angle airborne laser ranging system," *J. Opt. A*, vol. 1, pp. 77-82, 1999.
4. I. Fujima, S. Iwasaki, and K. Seta, "High-resolution distance meter using optical intensity modulation at 28 GHz," *Meas. Sci. Technol.*, vol. 9, pp. 1049-1052, 1998.
5. J. M. Payne, D. Parker, and R. G. Bradley, *Rev. Sci. Inst.*, vol. 63, pp. 3311-3316, 1992.

6. R. Dandliker, R. Tharlman, and D. Prongue, "Two-wavelength laser interferometry using super-heterodyne detection," *Opt. Lett.*, vol. 13, pp. 339-343, 1988.
7. J. A. Stone, A. Stejskal, and L. Howard, "Diode lasers in length metrology: application to absolute distance interferometry," *Cal Lab*, 1999.
8. D. Xiaoli and S. Katuo, "High-accuracy absolute distance measurement by means of wavelength scanning heterodyne interferometry," *Meas. Sci. Technol.*, vol. 9, pp. 1031-1035, 1998.
9. P. de Groot, "Three-color laser-diode interferometer," *Appl. Opt.*, vol. 30, pp. 3612-3616, 1991.
10. C. C. Williams and H. K. Wickramasinghe, "Absolute optical ranging with 200-nm resolution," *Opt. Lett.*, vol. 14, pp. 542-544, 1989.
11. X. H. Zhang, M.-C. Oh, A. Szep, W. H. Steier, Z. C, L. R. Dalton, H. Erlig, Y. Chang, D. H. Chang, and H. R. Fetterman, *Appl. Phys. Lett.*, vol. 78, pp. 3136, 2001.
12. R. N. Bracewell, "The Fourier Transform and its applications", McGraw-Hill, New York, 1986.
13. R. Hatch, "The Synergism of GPS Code and Carrier Measurements," Proceedings of 3rd International Geodetic Symposium on Satellite Doppler Positioning, DMA/NGS, pp. 1213-1232, Washington, D.C. (1982)
14. P. E. Ciddor, "Refractive index of air: new equations for the visible and near infrared." Appl. Optics 35, 1566-1573, 1996.
15. P. Halverson, D. Johnson, A. Kuhnert, S. Shaklan, R. Spero, "A multichannel averaging phasemeter for picometer precision laser metrology" *Proc. SPIE*, **3740**, 646-649 (1999).
16. A. Arie, M. L. Bortz, M. M. Fejer and R. L. Byer, "Iodine spectroscopy and absolute frequency stabilization with the second harmonic of the 1319-nm Nd:YAG laser", *Opt. Lett.*, **18**, 1757-1759, (1993)
17. V. S. Levtokov, "Saturation spectroscopy in high resolution laser spectroscopy," *Topics in Applied Physics*, **16** 849 (1991).
18. R.W.P. Drever, J. L. Hall, F. V. Kowalski, J. Hough, G. M. Ford, A. J. Munley, and H. Ward, "Laser Phase and Frequency Stabilization Using and Optical Resonator", *Appl. Phys. B,* **31**, 97 (1983).
19. National Institute of Standards and Technology website, Time and Frequency division, http://www.boulder.nist.gov/timefreq/